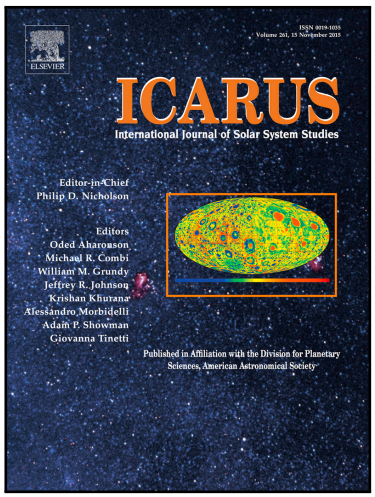

Dusk/Dawn Atmospheric Asymmetries on Tidally-Locked Satellites: O_2 at Europa

Apurva V. Oza, Robert E. Johnson, François Leblanc

PII: S0019-1035(17)30649-8
DOI: 10.1016/j.icarus.2017.12.032
Reference: YICAR 12752

To appear in: *Icarus*

Received date: 9 September 2017
Revised date: 13 November 2017
Accepted date: 20 December 2017

Please cite this article as: Apurva V. Oza, Robert E. Johnson, François Leblanc, Dusk/Dawn Atmospheric Asymmetries on Tidally-Locked Satellites: O_2 at Europa, *Icarus* (2017), doi: 10.1016/j.icarus.2017.12.032

Highlights

- A 1-D analytical model is presented to examine dusk/dawn asymmetries in tidally-locked satellites.
- The atmospheric shift towards dusk for a thermally-dependent source depends on the ratio between the rotation rate and the atmospheric loss rate.
- A simple thermally-dependent O_2 source is identified at Europa and possibly Ganymede.
- At Europa, the thermally-dependent O_2 source implies a large O_2 reservoir embedded in the porous ice.
- If this large O_2 reservoir exists it could be oxidizing the subsurface ocean as suggested by previous works.

DRAFT VERSION DECEMBER 28, 2017
Preprint typeset using LaTeX style AASTeX6 v. 1.0

DUSK/DAWN ATMOSPHERIC ASYMMETRIES ON TIDALLY-LOCKED SATELLITES: O_2 AT EUROPA

APURVA V. OZA[1], ROBERT E. JOHNSON[2] AND FRANÇOIS LEBLANC[1]

[1]LATMOS/IPSL, UPMC Univ. Paris 06 Sorbonne Universités, UVSQ, CNRS, Paris, France

[2]Engineering Physics, University of Virginia, Charlottesville, Virginia, USA

ABSTRACT

We use a simple analytic model to examine the effect of the atmospheric source properties on the spatial distribution of a volatile in a surface-bounded atmosphere on a satellite that is tidally-locked to its planet. Spatial asymmetries in the O_2 exosphere of Europa observed using the Hubble Space Telescope appear to reveal on average a dusk enhancement in the near-surface ultraviolet auroral emissions. Since the hop distances in these ballistic atmospheres are small, we use a 1-D mass conservation equation to estimate the latitudinally-averaged column densities produced by suggested O_2 sources. Although spatial asymmetries in the plasma flow and in the surface properties certainly affect the spatial distribution of the near-surface aurora, the dusk enhancements at Europa can be understood using a relatively simple thermally-dependent source. Such a source is consistent with the fact that radiolytically produced O_2 permeates their porous regoliths. The size of the shift towards dusk is determined by the ratio of the rotation rate and atmospheric loss rate. A thermally-dependent source emanating from a large reservoir of O_2 permeating Europa's icy regolith is consistent with the suggestion that its subsurface ocean might be oxidized by subduction of such radiolytic products.

1. INTRODUCTION

The near-surface, far-ultraviolet oxygen aurorae, observed for decades at Europa by the Hubble Space Telescope (Hall et al. (1995); Hall et al. (1998); McGrath et al. (2013) Roth et al. (2015)), appear to exhibit an enhancement in the emission intensity at the dusk observing longitudes as compared to the emission intensity seen at the dawn observing longitudes throughout Europa's orbit. A similar asymmetry was suggested by simulations at Ganymede (Leblanc et al. (2017)) yet to be clearly identified in the HST images (McGrath et al. (2013); Saur et al. (2015); Musacchio et al. (2017)). Although such asymmetries depend on the electron density and temperature, they also depend on the O_2 column density and could suggest that the O_2 column density in these thin atmospheres peak near dusk. If that is the case, this is opposite to what is seen for radiolytic argon on the Moon where peak column density occurs near dawn, due to its rapid release from the

apurva.oza@latmos.ipsl.fr

uppermost layer of the regolith after being condensed at night (Hodges & Hoffman (1974); Hodges et al. (1974); Grava et al. (2015)). Molecules in these atmospheres undergo frequent interactions with the surface such that the hop distances are typically much less than the planetary radius, and the ballistic hop time is much smaller than the volatile lifetime. Therefore, the volatiles respond primarily to the local surface properties and are typically assumed to be thermally accommodated to the local surface temperature. The stellar insolation of the local surface therefore should play a critical role in the shaping of the exospheres of these tidally-locked satellites, as was also recently evidenced *in-situ* by Cassini's INMS sampling of CO_2 & O_2 on Rhea and Dione Teolis & Waite (2016).

O_2 on the icy satellites of the outer planets have a far different origin than on Earth. These satellites are covered in water ice and are embedded in a gas giant's magnetosphere. The magnetic fields accelerate charged particles which bombard the surface and eject O_2, H_2, H_2O, as well as their dissociation products and trace species (e.g.,Leblanc et al. (2017)). This is often referred to as magnetospheric ion sputtering Johnson et al. (1982) with the production of O_2 and H_2 a result of chemical processes initiated in the ice by the incident charged particles, a process also known as radiolysis (Johnson 1990; Teolis et al. (2017) *in press*). Laboratory studies indicate that the product yields have a strong thermal dependence when ejected from the ice which is also the case when they are absorbed and re-emitted. In this way the spatial distribution of the radiolytically produced O_2 can, in principle, depend strongly on the local surface temperature. Therefore, the near-surface O_2 atmosphere is capable of directly responding to the stellar insolation.

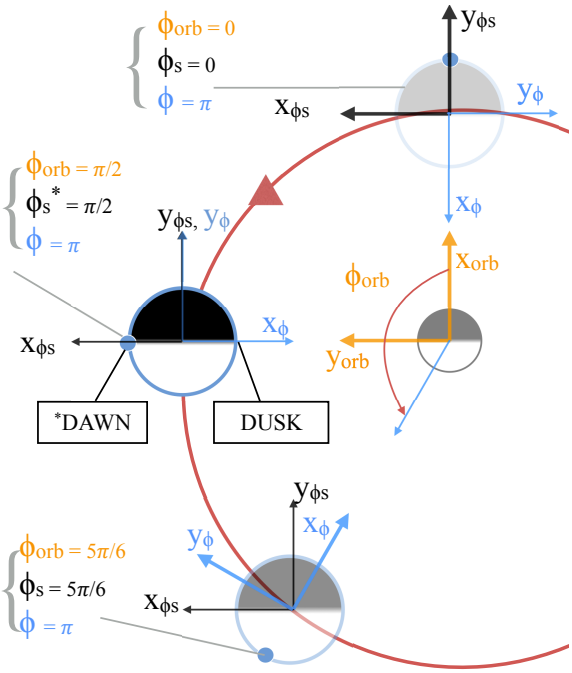

Figure 1. Satellite coordinate system for a rotating satellite at two positions with respect to its parent planet at the center. Black vectors represent the fixed, observers frame, where y_{ϕ_s} in black indicates the incoming solar radiation flux vector. ϕ_s is the anti-stellar insolation vector, defined as such in order to synchronize the two frames, where Dusk: $\phi_s = 3\pi/2$ and Dawn: $\phi_s = \pi/2$. Blue vectors represent the rotating, satellite frame where ϕ is the satellite longitude whose origin is the subplanetary point. We define the origin of the satellite system (blue circle) as $\phi_0 = \phi + \pi$ to effectively compare to observations such that the subobserver longitude is synchronized with the planetary longitude at midnight during satellite eclipse. In a time Δt, the satellite will have rotated a $\Delta\phi_{obs} = \Omega\Delta t$.

As the auroral process is complex, involving the production, loss, transport and excitation rates, we focus here on the role of the O_2 source rate. Therefore, we construct atmospheres using a simple analytic model for a number of possible sources driven by the stellar insolation and the magnetospheric plasma bombardment.

2. ATMOSPHERIC EVOLUTION MODEL

Here we describe the orbital evolution of the local exospheric column density on a tidally-locked satellite. Its morphology depends on the spatial distributions of the source and loss rates as well as on the satellite's rotation rate Ω. For the satellites considered the diffusion time across the surface is longer than the volatile's lifetime and their average thermal hop distance is much less than the planetary radius simplifying the analysis. For a satellite of mass m_s, radius r_s, synchronously rotating about a planet of mass M_p, a distance a_s away, the rotation rate is $\Omega = (\frac{GM_p}{a_s^3})^{1/2}$ with an orbital period $\tau_{orb} = \frac{\Omega}{2\pi}$. The rotation produces both centrifugal and Coriolis forces, treated in detail in 3-D Monte Carlo simulations (Oza et al. (2017); Leblanc et al. (2017)), which we initially ignore but discuss later. Figure 1 illustrates our equatorial coordinate system, where the stellar flux is fixed and arrives from the bottom of the page, along the radiation vector y_{ϕ_s} (black vertical line). The inertial reference frame is represented by the black vectors indicating the time in the planet-satellite system defined by the anti-stellar insolation angle ϕ_s, where midnight corresponds to 0 and the substellar point is at π. The sub-observer longitude ϕ_{orb} (orange axes) is the star-planet-satellite angle and keeps track of the satellite's rotation around the planet. Because the satellite is phase-locked to its parent planet, it is also the longitude on the body with respect to the plasma ram along the corotation axis ϕ' (red). The satellite's rotational reference frame (blue axes) is the longitude measured counter-clockwise with its origin at the subplanetary point where $\phi = \phi' + \frac{\pi}{2}$. As we will integrate over time, we will use an origin synchronizing these reference frames. If we begin by evaluating the anti-planetary point, $\phi = \pi$, represented by the blue dot at midnight, $\phi_{orb} = \phi_s = 0$, then the observer's clock is synchronized with the satellite's clock. Therefore, in a time interval t, the satellite rotates about its axis such that $\phi_{orb} = \Omega t$. The translation between the inertial and non-inertial reference frames is $\phi_s = \phi_{orb} + \phi - \pi = \Omega t + \phi - \pi$. Hence, after a time $\frac{\tau_{orb}}{4}$, the satellite arrives at the *sunlit* leading hemisphere corresponding to $\phi_{orb} = \pi/2$ for the observer, and $\phi_s = \pi/2$ corresponding to dawn local time as indicated in Figure 1. By rotating an additional $\tau_{orb}/6$, the fixed blue points on the satellite rotate towards substellar so that in Figure 1: $\phi_s = 5\pi/6$. Lastly, not shown in the figure is the blue point reaching the *sunlit* trailing hemisphere orbital longitude where $\phi_{orb} = 3\pi/2$ and $\phi_s = 3\pi/2$ corresponding to dusk local time. Since our interest is in the longitudinal variation (e.g., dusk/dawn asymmetries), we consider a latitudinally averaged column of gas, N. For a given source, the atmosphere reaches approximate steady-state after a number of orbits, such that the source flux, Φ, balances the loss flux νN. Here ν is the loss rate which can depend on the longitude ϕ through the local properties of the plasma and on the stellar flux $\Phi_T(\phi_s)$. Writing the rate of change of N as a simple balance between an atmospheric source and loss rate, the orbital evolution is determined from

$$\frac{dN(\phi,t)}{dt} = \Phi(\phi,\phi_s) - \nu(\phi,\phi_s)N(\phi,t) \quad (1)$$

As the parameter space is large, we assume that the variations in loss rate are much smaller than those in the source

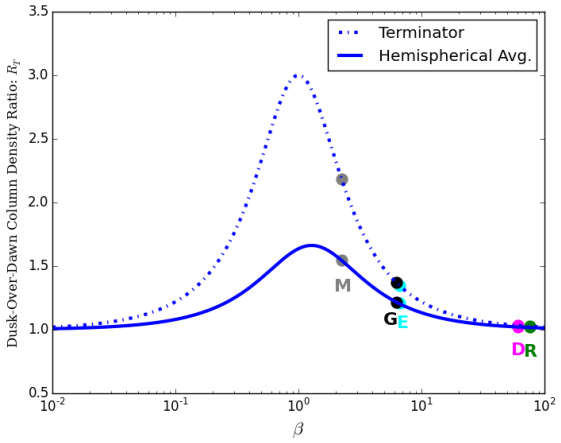

Figure 2. Dusk-over-dawn asymmetry ratio, R, versus $\beta = \Omega/\nu$ for the thermal source in Eqn. 3. For $\Omega \sim \nu$ the asymmetry is a maximum. The dash-dotted blue line roughly represents the terminator ratio following Eqn. 6 whereas the solid blue line is the hemispherical average of the ratio following Eqn. 7. The circles represent various satellites from Table 1: cyan & black are the Galilean satellites Europa (E) and Ganymede (G) respectively. The magenta & green points are the Saturnian satellites Dione (D) and Rhea (R) respectively. The gray point is the Moon (M) to demonstrate Lunar argon's natural tendency to peak at dusk-over-dawn should there be negligible condensation and diffusion.

distribution. By assuming that ν is roughly constant in space and time (e.g., Saur et al. (2011), we focus on the role of the source in determining the distribution of gas across the surface. In this case, the solution to Eq.1 is

$$N(\phi,t) = exp(-\nu t)\left(\int_0^t exp(\nu t')\Phi(\phi,\phi_s)dt' + N(\phi)_0\right) \quad (2)$$

where $N(\phi)_0$ is the initial column density of the gas at time, $t = 0$. In this approximation, the latitudinal distribution of the radial column density from Eqn. 2 is determined by primarily the source, Φ.

An asymmetry in N between the dusk and dawn terminators ($\phi_s = 3\pi/2;\ \pi/2$ respectively) can be shown by the ratio of their column densities, R. For $R > 1$, N is larger toward dusk. Since the difference in the scale heights is small, R is roughly proportional to the line-of-sight (LOS) column densities at the terminators. Because remotely observed LOS emission intensities probe the sunlit hemispheres, we also compute a hemispherically-averaged ratio, $\langle R \rangle$, ignoring the small contribution at the terminators from the nightside atmosphere. Averaging N across longitude on the dusk quadrant, $\phi_s = \pi \rightarrow 3\pi/2$, $\langle N_{DUSK} \rangle$, and the dawn quadrant, $\phi_s = \pi \rightarrow \pi/2$ $\langle N_{DAWN} \rangle$ we calculate a ratio that can be more readily compared to the observations.

Below we use three source functions that have been discussed. For each we derive the column density as a function of ϕ and t, first computing R, the dusk/dawn ratio and then the hemispherically averaged ratio, $\langle R \rangle$. These are then discussed based on the observed auroral emission ratios.

2.1. *Solar Radiation-Driven Source*

We first consider a source solely dependent on the stellar insolation. As an example, we construct a simple sublimation-like source that only depends on ϕ_s and peaks at noon

$$\Phi_T(\phi_s) = \frac{\Phi_0}{2}\,(1 - cos(\phi_s)) \quad (3)$$

where Φ_0 is the maximum flux. Substituting into and integrating Eqn. 2 we obtain

$$N_T(\phi,t) = \frac{\Phi_0}{2\nu}\left([1 - exp(-\nu t)] - N_{rot}(\phi_s,t)\right) \quad (4)$$

Writing $\beta = \Omega/\nu$ and $\alpha = \phi - \pi$, then $N_{rot}(\phi_s,t) = (1 + \beta^2)^{-1}\left([cos(\phi_s) + \beta sin(\phi_s)] - [cos(\alpha) + \beta sin(\alpha)]exp(-\nu t)\right)$. As $t \rightarrow \infty$, the spatial distribution of the steady-state column density is seen to depend solely on the stellar insolation angle ϕ_s giving

$$N_T(\phi) = \frac{\Phi_0}{2\nu}\left(1 - (1+\beta^2)^{-1}[cos(\phi_s) + \beta sin(\phi_s)]\right) \quad (5)$$

The ratio R_T, the dusk-over-dawn column densities evaluated at the terminators, is

$$R_T \sim \frac{1 + \beta + \beta^2}{1 - \beta + \beta^2}. \quad (6)$$

corresponding to the dashed blue curve shown in Figure 2. Because Φ_0 cancels, it is seen that for such a source with roughly constant loss rate, R_T is greater than unity and depends only on the ratio β. In this approximation the maximum column density occurs past noon simply due to the rotation of the source peak towards dusk (e.g., Hodges & Johnson (1968)). As seen in Oza et al. (2017) for Europa, the peak temperature actually occurs just past noon so that the shift towards the dusk terminator would be somewhat larger.

The dusk/dawn ratio averaged over the the half-hemispheres is

$$< R_T >= \frac{1 + \frac{2}{\pi}(\beta + 1) + \beta^2}{1 - \frac{2}{\pi}(\beta - 1) + \beta^2} \quad (7)$$

which is given by the solid blue curve in Figure 2. The values of β in Table 1 for the various satellites are indicated by colored dots. It can be seen that for the assumed source and loss process, the atmospheres of Europa and Ganymede would possess column densities which are at least 50 % thicker at dusk than at dawn. For the Saturnian satellites the loss rates are roughly a factor of 10 smaller (Table 3; Teolis & Waite (2016)) consistent with the absence of a dusk-over-dawn asymmetry.

2.2. *Magnetospherically-Driven Source*

Icy satellite O_2 exospheres embedded in large planetary magnetospheres are thought to be generated by plasma flow along the satellite's orbit. Such a source depends on the satellite corotation direction. Since the plasma has a thermal and an energetic component, and the ions have gyromotion determined by their energy and the local fields, how strongly the O_2 source peaks at plasma ram direction has been discussed (e.g., Cassidy et al. (2013).; Teolis et al. (2005)). Here we only assume the source rate is a function of the angle from the corotation and can be approximated as:

$$\Phi(\phi)_{mag} = \frac{\Phi_0}{2}\left(1 + sin(\phi)\right) \quad (8)$$

Again assuming a nearly constant loss rate, Eqn. 2 yields, not surprisingly, an expression with no rotational term

$$N_{mag}(\phi) = \frac{\Phi(\phi)_{mag}}{\nu}\left([1 - exp(-\nu t)]\right) \quad (9)$$

Therefore, rather than an enhancement at dusk over the full orbit, the dusk-over-dawn ratio oscillates with an orbit average R of about one.

S	τ_{orb} [hrs]	τ_i [hrs] (τ_{orb})	β	R_T	$\langle R_T \rangle$
E	85	90 (1.06)	6.78	1.34	1.20
G	172	170 (1.0)	6.28	1.37	1.22
D	66	604 (9.2)	61	1.03	1.02
R	108	1262 (12)	77	1.02	1.02
M	656	2669 (4.1)	2.3	2.18	1.54

Table 1. Atmospheric evolution parameters and values for the various surface-bounded satellite exospheres described in Figure 2. τ_{orb} is the orbital period in hours, τ_i the atmospheric lifetime of the species i in question, scaled to the orbital period in parentheses. $\beta = \frac{\Omega}{\nu}$ a parameter indicating the magnitude of the asymmetry, depending only on the rotational rate of the satellite Ω and the atmospheric loss rate ν. The loss rates for Europa and Ganymede are calculated from photon and electron ionization and dissociation rates provided in Turc et al. (2014) Table 2, for an isotropic electron density of $n_e = 70cm^{-3}$ (e.g. Marconi (2007)). Dione and Rhea's O_2 loss rates are estimated by Teolis & Waite (2016) Table 3, whereas the Lunar argon loss rate Grava et al. (2015) Table 1. R_T and $\langle R_T \rangle$ are the latitudinally averaged dusk-over-dawn ratios for a satellite with a radiation-driven source estimated using Eqn. 6 (evaluated at the terminator) and Eqn. 7 (hemispherically-averaged) respectively.

2.3. *Solar Radiation & Magnetosphere-Driven Source*

Laboratory data indicate that the plasma-induced source of O_2 depends on the ice temperature. Although it has been argued that on the icy satellites this dependence is averaged out due to delayed emission of the O_2 (Teolis et al. (2005)), a predominately trailing hemisphere source $\Phi(\phi)_{mag}$ with a thermal enhancement has been used often (e.g., Cassidy et al. (2007); Plainaki et al. (2012); Plainaki et al. (2013); Oza et al. (2017)). Here we roughly represent such a source by:

$$\Phi(\phi,\phi_s)_{Tmag} = \frac{\Phi_0}{2}(1+sin(\phi)) * [3 - cos(\phi_s)]/2 \quad (10)$$

This results in a steady-state column

$$N_{Tmag}(\phi) = \frac{\Phi(\phi)_{mag}}{2\nu}\left(3 - \frac{1}{1+\beta^2}(cos(\phi_s) + \beta sin(\phi_s))\right) \quad (11)$$

Based on the above expression, the rotation shifts the maximum and minimum column densties from noon and midnight by $tan^{-1}(\beta)$. For Europa and Ganymede, with β values near 2π, this shift corresponds to $\sim 81°$. In satellite local time, the column increases from its minimum value near dawn, ~ 6h30, to its maximum column near dusk, ~ 17h30. The magnitude of the dusk-over-dawn asymmetry at the terminators is

$$R_{Tmag} = \frac{1 + \beta/3 + \beta^2}{1 - \beta/3 + \beta^2} \quad (12)$$

The ratio of the averaged column densities, $< R >$, results in a more complex expression and is given in Table 2 at a few orbital positions. It is seen that although R_{Tmag} in Eqn. 12 is greater than one, the averaged ratio is not always greater than one and varies significantly from the sunlit leading hemisphere to the sunlit trailing hemisphere.

3. ICY SATELLITE O_2 ATMOSPHERES

Although variations on these overly simplified source terms have been used, here we compare the predicted ratios. We start by considering Europa for which its near-surface

oxygen aurorae observations are the most complete. Since the O_2 exosphere is produced radiolytically by the incident plasma, uncertainties regarding the production, loss, and excitation rates, as well as the O_2 residence in the regolith, have been an obstacle in describing the observed emission asymmetries. Focusing here on the source process, values of R and $< R >$ are given in Table 2 for the above three cases at four orbital positions: sunlit trailing eclipse, sunlit leading, and substellar. Also shown are the ratios obtained from the HST observations.

These results are also shown in Figure 3 where they are compared to the HST observations (black points) in order to illustrate the effect of the source process on the near surface aurora. Also shown are the Monte Carlo simulations of Europa's exosphere from Oza et al. (2017) for a thermally-dependent sputter source (EGM sim.; blue points). Such simulations account for diffusive hopping as well as the centrifugal and Coriolis forces. It is seen that the observed dusk/dawn emission ratio does not vary significantly over an orbit. In contrast to that, the simulations in Oza et al. (2017) and the magnetosphere models ($\langle R \rangle_{mag}$; $\langle R \rangle_{Tmag}$) differ significantly from the observed emission ratio. It is also clear that a temperature-independent magnetospheric sputter source, suggested by the delay times in the O_2 emission (Teolis et al. (2017)) and roughly approximated here by Eqn. 8, would not by itself give the observed dusk/dawn ratio. The lack of agreement of the observations with detailed simulations in Oza et al. (2017) and with the approximate magnetospheric sources suggests that the direct use of the laboratory measurements could be problematic. The comparison with the simulations improves somewhat by accounting for the O_2 residence time in Europa's regolith (Oza et al. (2017)). And, of course, significant spatial variations in the plasma-induced loss and in

ϕ_{orb}	$\langle R(T)_{EGM} \rangle$	$\langle R \rangle_{mag}$	$\langle R(T) \rangle_{Tmag}$	$\langle R_{HST} \rangle$
270	1.58	1.0	1.06	1.64 ±0.14
0	1.35	4.5	4.8	1.73 ±0.7 ; 1.53 ±0.2
90	6.87	1.0	1.09	1.29 ±0.1
180	6.06	0.22	0.24	1.57 ±0.2 ; 1.92 ±0.2

Table 2. Dusk/Dawn ratios of atmospheric O_2 bulges on Europa, calculated as hemispherically averaged column-density ratios $\langle R \rangle \sim N_{Dusk}/N_{Dawn}$ over the four major orbital phases: sunlit trailing (270), eclipse (0), sunlit leading (90), and substellar (180). The fixed sublimation source maintains a constant dusk-over-dawn asymmetry of: $< R_T >$ = 1.2 for all orbital longitudes. The four R columns represent the latter two magnetospheric plasma cases in section §2.2, and 2.3. The second column is the EGM output of Oza et al. (2017) for a non-adsorbing, thermally-dependent O_2 case. The final column is the average auroral intensity ratio, I_{Dusk}/I_{Dawn}, observed by HST at 1356 $\AA$ potentially indicative of the exospheric asymmetry. The HST eclipse values are averaged around a ~ 23° interval in orbital longitude, whereas the substellar values are averaged around a larger ~ 100° interval. For these latter two cases we provide pre and post transit values.

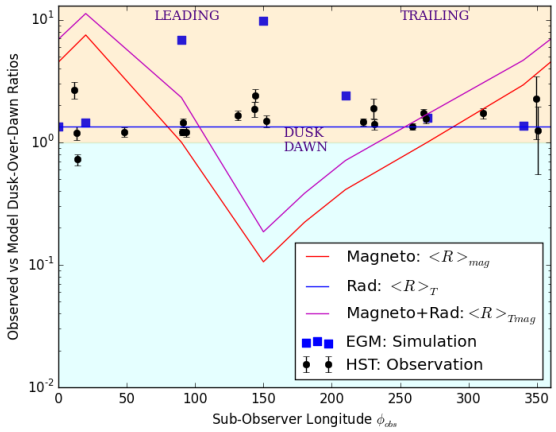

Figure 3. Average dusk-over-dawn asymmetry ratio, $\langle R \rangle$, versus sub-observer longitude ϕ_{orb} indicating dusk enhancements shaded in orange, and dawn enhancements in blue. The 3-D Monte Carlo exosphere simulations from Oza et al. (2017) representing a non-adsorbing O_2 population (blue squares) as well as the oxygen emission data from Roth et al. (2015) by HST (black points) dominate the dusk-enhanced region. Our three source cases: radiation-driven ($\langle R \rangle_T$) , magnetospherically-driven ($\langle R \rangle_{mag}$), and a temperature-enhanced version of the radiation & magnetospherically-driven ($\langle R \rangle_{Tmag}$) O_2 sources are represented by the solid blue, red, and magenta lines respectively. It can be seen that only the stellar radiation-driven O_2 source provides a reasonable fit to the HST observations.

the excitation rates could further improve these comparisons.

What is striking about the comparison in Fig. 3 is that the ratio obtained for the hemispherically averaged O_2 sublimation source (blue line), as in Eqn. 3, gives a result that is surprisingly close to that observed. Since the O_2 is beyond doubt produced by the impacting plasma this comparison could suggest that there is indeed a temperature-dependent source rate. However, the rate is not like that modeled by a direct use of the laboratory data, roughly approximated here in Eqn. 10 or treated in much more detail in the simulations. Since the residence time in the regolith of the returning O_2 clearly has an effect Oza et al. (2017), we suggest the agreement is likely due to the fact that the O_2 produced over geological time periods permeates the regolith on Europa (e.g.,Johnson et al. (2003);Hand et al. (2007); Greenberg (2010);Teolis & Waite (2016)). If that is the case, then the direct production rate, whether enhanced on the trailing hemisphere or thermally-dependent, contributes marginally per orbit to a large reservoir of O_2 bound in the regolith. This O_2 likely exhibits a rough vapor pressure equilibrium determined by its binding in the porous icy regolith. Magnetospheric-ion production acting over long time periods should result in a significant amount of O_2 trapped in the ice which is able to thermally diffuse and populate the exosphere. In this model the maximum in the O_2 atmospheric source is shifted by the satellite rotation generating an asymmetric atmosphere that peaks toward dusk.

The highly simplified model presented here does not account for O_2 transport, although it has been included in the 3-D exosphere simulations (e.g., Leblanc et al. (2017); Oza et al. (2017)). Latitudinal transport is strongly suggested by the observation of equatorial O_2 bulges throughout Ganymede's orbit (Leblanc et al. (2017)). That is, O_2 is produced primarily in the polar regions (McGrath et al. (2004)) but is found to have migrated towards the equator on orbital timescales (Leblanc et al. (2017)). This latitudinal motion

is driven by the centrifugal force treated in the simulations but ignored here. The primary effect of this transport is very roughly accounted for here by latitudinally-averaging the O_2 column densities.

4. CONCLUSION & SUMMARY

Because numerous processes affect the auroral observations of the exospheres at Europa and Ganymede, we used a simple analytic model to focus on the asymmetry produced only by the atmospheric source. In doing this we assumed that the effect of the spatial asymmetries in both the plasma-induced loss and the auroral excitation rates are much smaller than those produced by the source. Although this is a significant assumption, at present it does not contradict models of ionization and excitation rates which depend on both the local electron density and temperature. In addition, we ignored thermal transport, as the molecular hop distances were small compared to the satellite radius so that the latitudinally averaged column is very roughly synchronized with the surface rotation. It is seen that for Europa a plasma-induced source enhanced on the trailing hemisphere, whether thermally dependent or not, does not produce spatial asymmetries consistent with the emission observations. That comparison could, of course, be considerably improved by the presence of a significant spatial variation in the plasma-induced loss and emission rates. However, the orbital dependence of the half hemisphere average of the dusk/dawn emission ratio at Europa is seen to compare favorably with a simple thermal dependent, solar heating source on these tidally locked icy satellites. This might also be the case at Ganymede, although the observations are less extensive and its magnetic field can complicate the comparison. The magnitude of the shift towards dusk produced by such a source was seen to depend on the ratio of the rotation rate to the loss rate, in addition to any shift in the thermal peak towards dusk as seen in Fig. 5 in Oza et al. (2017). Although the comparison could be fortuitous we note that such a source is not unreasonable. That is, the O_2 produced over long time periods likely permeates the porous icy regolith, even to the point where it has been suggested that it is a viable source of O_2 for Europa's ocean (e.g. Johnson et al. (2003); Hand et al. (2007); Vance et al. (2016)), so that the daily varying production is a small fraction of the available O_2. Therefore, we suggest that the thermally desorbed O_2 populates the atmosphere at a rate that primarily depends on the local temperature and its binding properties in these porous regoliths. Since the well known hemispherical differences in composition and albedo affect both the surface temperature and the binding we suggest these are secondary effects, a point that needs further testing. Of course, spatial differences in the local source rate will exist at smaller spatial scales than that considered due to the variation in the local surface properties and indeed, in the absence of averaging over the half hemispheres, the observations indicate such spatial variations. While the mechanism that generates the O_2 atmosphere on the icy satellites has been identified, namely plasma-driven production, a good simulation of the *orbital* observations is still not available. Here we suggest that lack of agreement might be due to the assumptions about the na-

ture of the O_2 source. If the observed O_2 is indeed due to the presence of a large reservoir, the mechanism suggested for oxidizing Europa's subsurface ocean, Johnson et al. (2003), Hand et al. (2007) may be more credible.

Acknowledgments: The authors acknowledge helpful comments from Dr. T.A. Cassidy. AVO and FL would like to acknowledge LabEx/ESEP for their support, as well as the CNES Système Solaire program. REJ acknowledges support from NASA's Planetary Data Systems Program.

REFERENCES

Cassidy, T. A., Johnson, R. E., McGrath, M. A., Wong, M. C., & Cooper, J. F. 2007, Icarus, 191, 755
Cassidy, T. A., Paranicas, C. P., Shirley, J. H., et al. 2013, Planet. Space Sci., 77, 64
Grava, C., Chaufray, J.-Y., Retherford, K. D., et al. 2015, Icarus, 255, 135
Greenberg, R. 2010, Astrobiology, 10, 275
Hall, D. T., Feldman, P. D., McGrath, M. A., & Strobel, D. F. 1998, ApJ, 499, 475
Hall, D. T., Strobel, D. F., Feldman, P. D., McGrath, M. A., & Weaver, H. A. 1995, Nature, 373, 677
Hand, K. P., Carlson, R. W., & Chyba, C. F. 2007, Astrobiology, 7, 1006
Hodges, R. R., Hoffman, J. H., & Johnson, F. S. 1974, Icarus, 21, 415
Hodges, Jr., R. R., & Hoffman, J. H. 1974, in Lunar and Planetary Science Conference Proceedings, Vol. 5, Lunar and Planetary Science Conference Proceedings, 2955
Hodges, Jr., R. R., & Johnson, F. S. 1968, J. Geophys. Res., 73, 7307
Johnson, R. E. 1990, Energetic Charged-Particle Interactions with Atmospheres and Surfaces, 84
Johnson, R. E., Lanzerotti, L. J., & Brown, W. L. 1982, Nuclear Instruments and Methods, 198, 147
Johnson, R. E., Quickenden, T. I., Cooper, P. D., McKinley, A. J., & Freeman, C. G. 2003, Astrobiology, 3, 823
Leblanc, F., Oza, A. V., Leclercq, L., et al. 2017, Icarus, 293, 185
Marconi, M. L. 2007, Icarus, 190, 155
McGrath, M. A., Jia, X., Retherford, K., et al. 2013, Journal of Geophysical Research (Space Physics), 118, 2043
McGrath, M. A., Lellouch, E., Strobel, D. F., Feldman, P. D., & Johnson, R. E. 2004, Satellite atmospheres, ed. F. Bagenal, T. E. Dowling, & W. B. McKinnon, 457
Musacchio, F., Saur, J., Roth, L., et al. 2017, Journal of Geophysical Research (Space Physics), 122, 2855
Oza, A., Leblanc, F., Johnson, R., et al. 2017, submitted
Plainaki, C., Milillo, A., Mura, A., et al. 2012, Icarus, 218, 956
—. 2013, Planet. Space Sci., 88, 42
Roth, L., Saur, J., Retherford, K. D., et al. 2015, J. Geophys, 261, 1
Saur, J., Feldman, P. D., Roth, L., et al. 2011, ApJ, 738, 153
Saur, J., Duling, S., Roth, L., et al. 2015, Journal of Geophysical Research (Space Physics), 120, 1715
Teolis, B., Plainaki, C., Cassidy, T., & Raut, U. 2017, in Press
Teolis, B. D., Vidal, R. A., Shi, J., & Baragiola, R. A. 2005, Phys. Rev. B, 72, 245422
Teolis, B. D., & Waite, J. H. 2016, Icarus, 272, 277
Turc, L., Leclercq, L., Leblanc, F., Modolo, R., & Chaufray, J.-Y. 2014, Icarus, 229, 157
Vance, S. D., Hand, K. P., & Pappalardo, R. T. 2016, Geophys. Res. Lett., 43, 4871